

Figure S1. Precise and robust gene expression profiling by our optimized snRNA-seq protocol. (A) Gene expression analysis of adipocyte and immune/endothelial cell markers in adipocyte and non-adipocyte nuclei ($n=3$, each) from eWAT of NuTRAP mice, utilizing the optimized protocol with VRC. Data are presented as mean \pm SEM, and statistical analysis was performed using Student's t test. * $p < 0.05$, ** $p < 0.01$, *** $p < 0.001$. (B) Sequential gating strategies for fluorescence-activated nucleus sorting (FANS) used to sort all Hoechst-positive

nuclei from adipose tissue for snRNA-seq. **(C-D)** Exemplary profiles of **(C)** cDNA and **(D)** sequencing library fragment size distribution, assessed by Agilent Bioanalyzer and TapeStation, respectively. **(E)** Levels of ambient RNA in the samples of this study (left) and Emont et al. (GSE176171, right), examined using CellBender. The plots describe both the rank-ordered UMI counts per droplet (represented by a black line) and the probabilities of each droplet containing a cell (indicated by red dots with dashed lines).

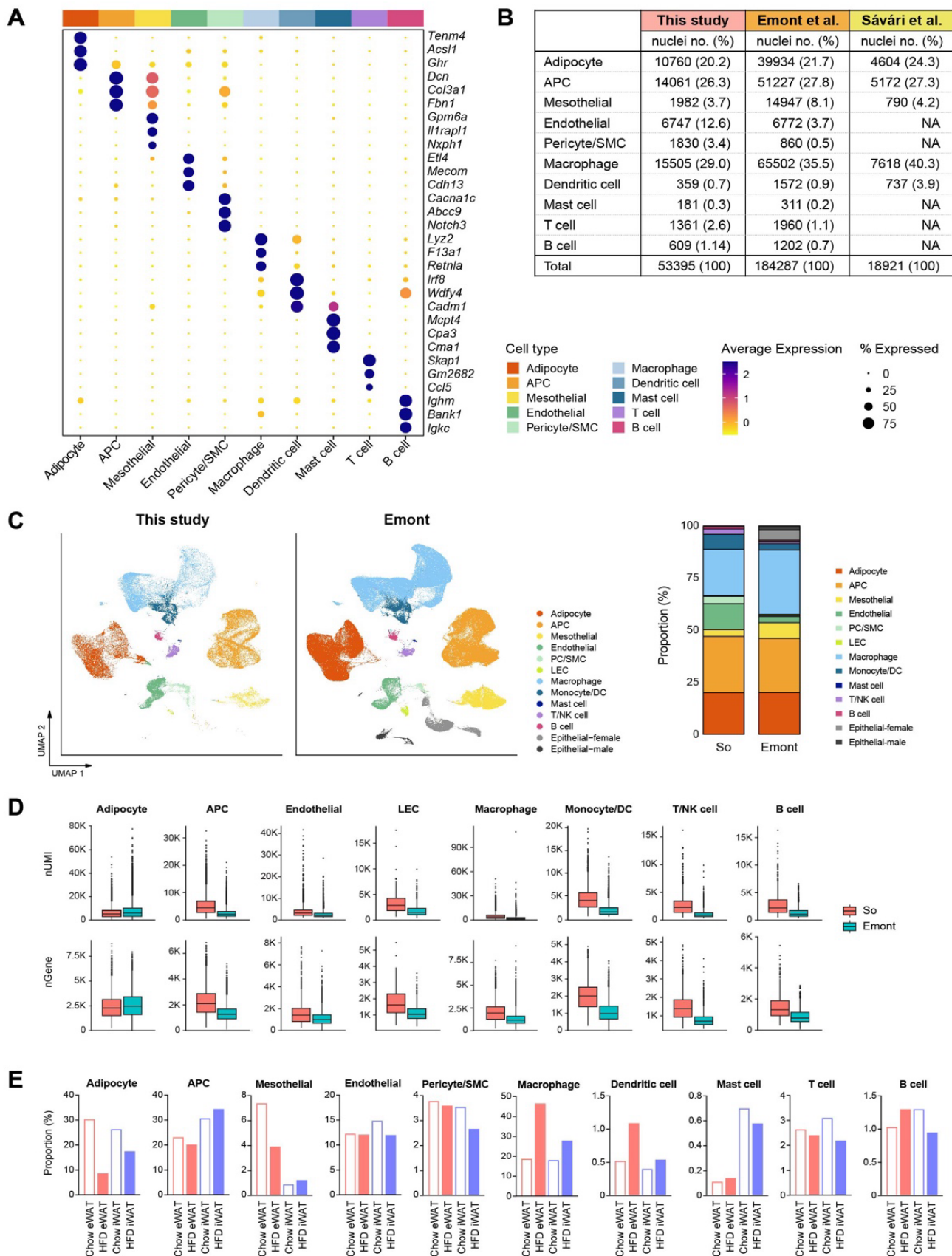


Figure S2. Profile of our single nucleus atlas encompassing diverse cell populations. (A)

Dot plots showing average scaled expression of the top three cell type marker genes in each cell population in mouse adipose tissue. **(B-D)** Comparison of mouse adipose tissue snRNA-seq data from this study with data from previous snRNA-seq studies. **(B)** The absolute numbers and relative proportions of nuclei recovered for each cell type. **(C)** Integration of all cell types from this study with those from Emont *et al.* Bar graphs on the right side display the relative proportions of individual cell types in each dataset. **(D)** Comparison of UMI counts and genes detected per nucleus by cell type between this study and Emont *et al.* **(E)** Bar graphs showing the relative proportions of individual cell types by fat depot and diet in this study.

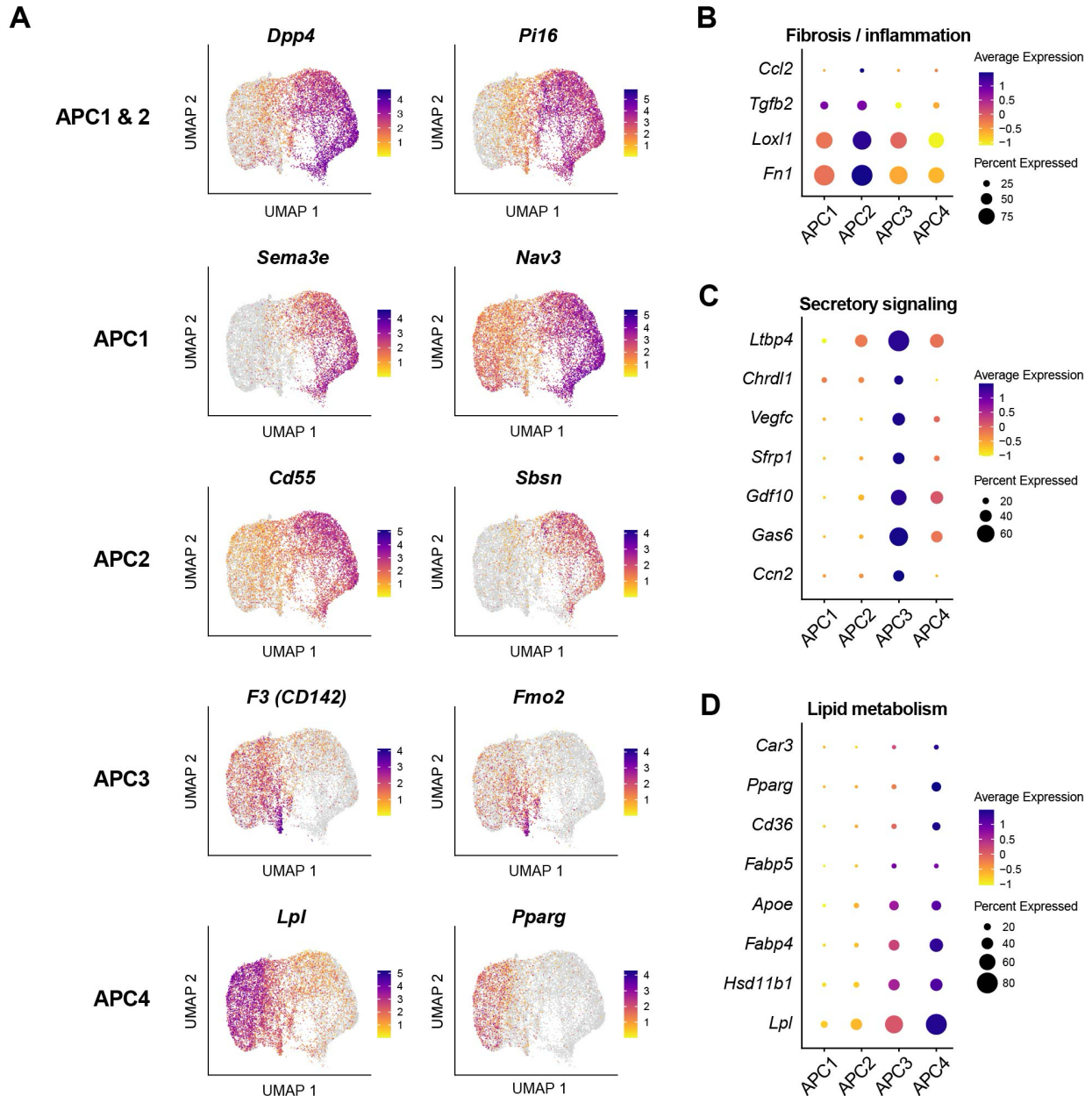


Figure S3. Gene expression profiles of APC subpopulations indicating distinct functional states. (A) UMAP visualization of marker genes for APC subpopulations. **(B-D)** Dot plots showing the expression of genes associated with fibrosis/inflammation **(B)**, secretory signaling **(C)**, and lipid metabolism **(D)** across APC subpopulations.

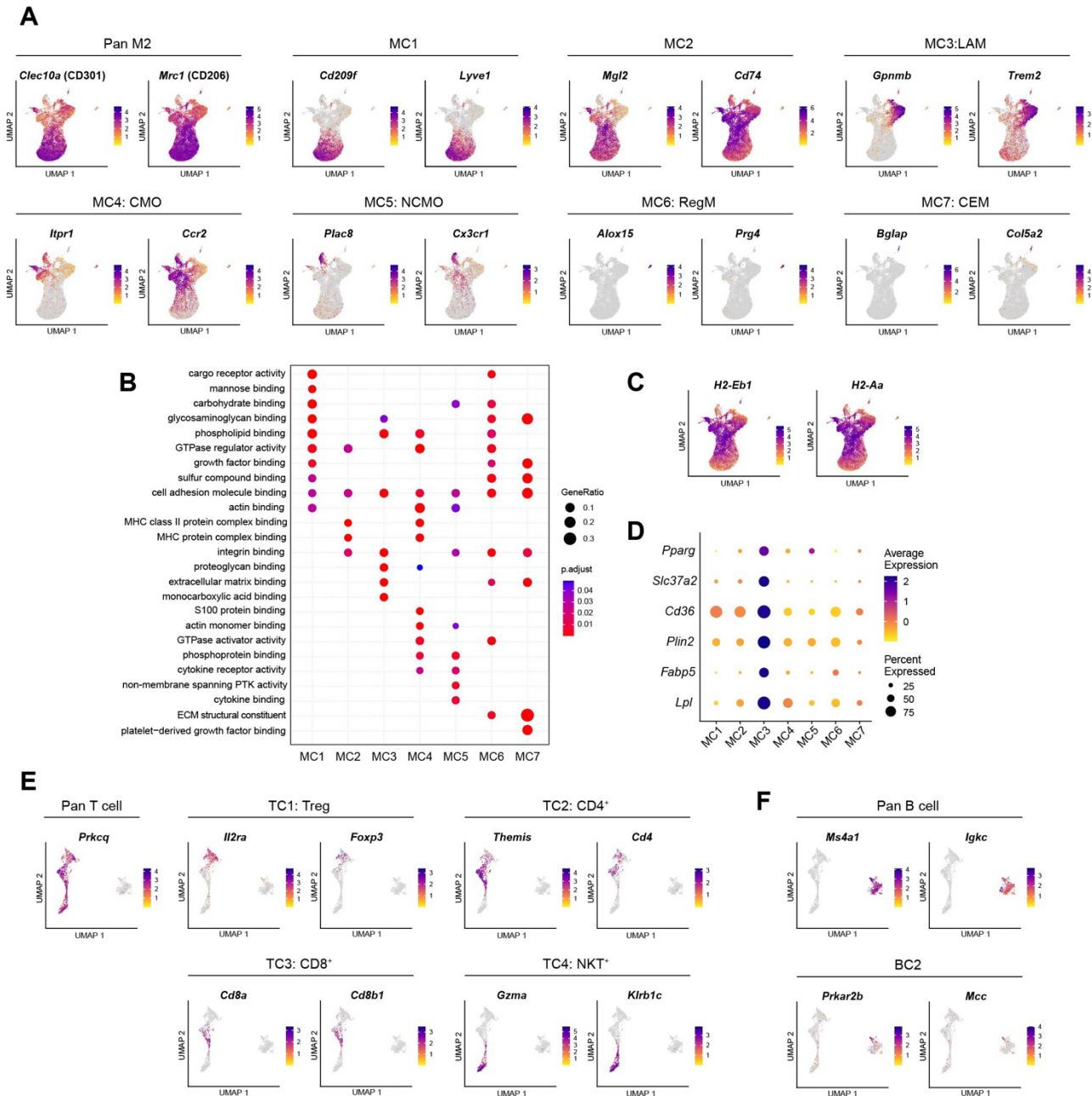


Figure S4. Characterization of diverse immune cell subpopulations. (A) UMAP visualization of marker genes for macrophage/monocyte subpopulations. **(B)** Dot plot illustrating pathways enriched within the top 100 marker genes of macrophage/monocyte subpopulations, as determined by clusterProfiler. **(C)** UMAP visualization of major histocompatibility complex (MHC) genes in macrophage/monocyte subpopulations. **(D)** Dot plot showing the expression of genes associated with lipid metabolism across macrophage/monocyte subpopulations. **(E)** UMAP visualization of marker genes for lymphocyte subpopulations.

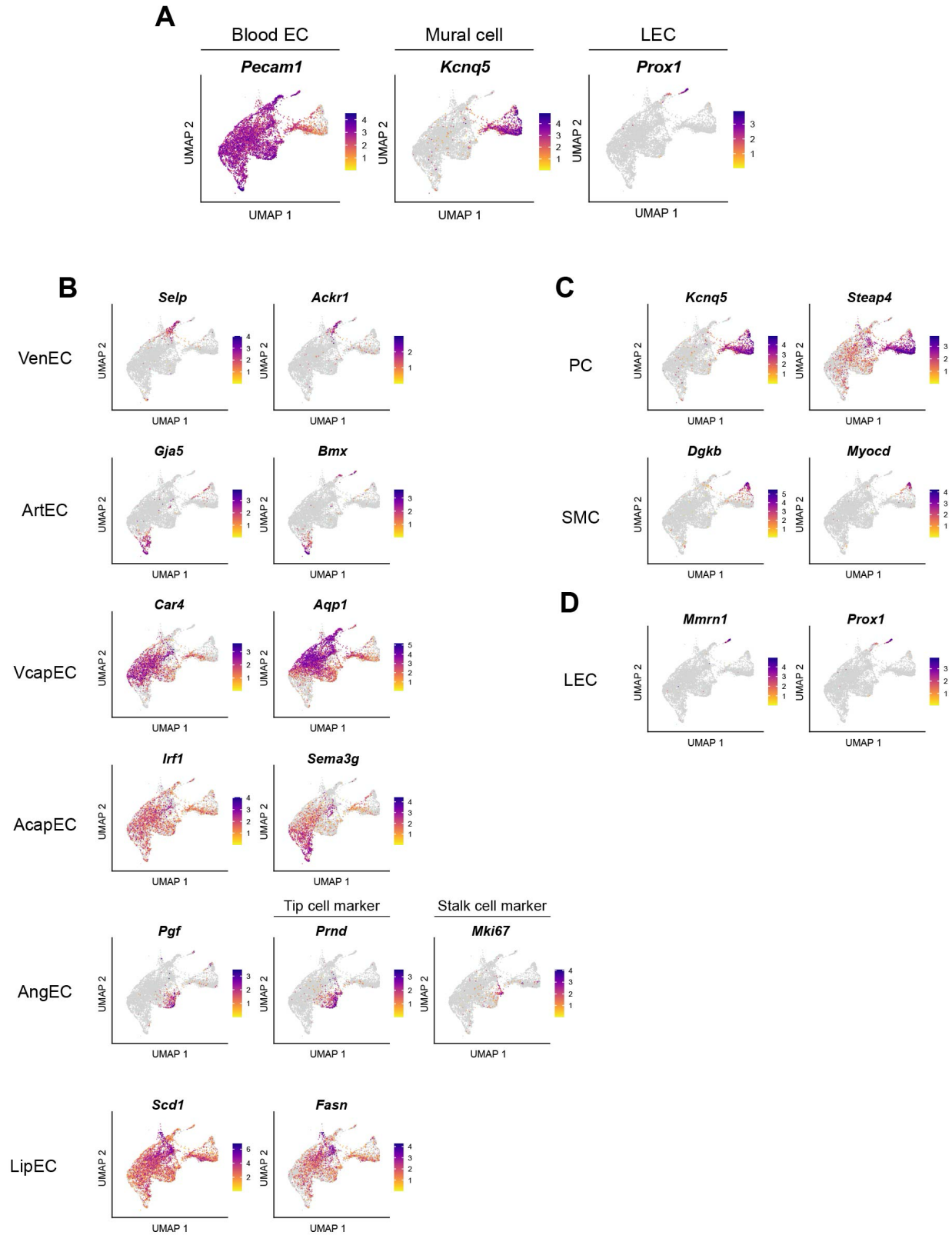


Figure S5. Characterization of diverse vascular cell subpopulations. (A) UMAP visualization using *Pecam1* for blood EC, *Kcnq5* for mural cells, and *Prox1* for LEC within vascular cells. **(B-D)** UMAP visualization of marker genes for **(B)** blood EC subpopulations. **(C)** mural cell subpopulations, and **(D)** LEC subpopulation.

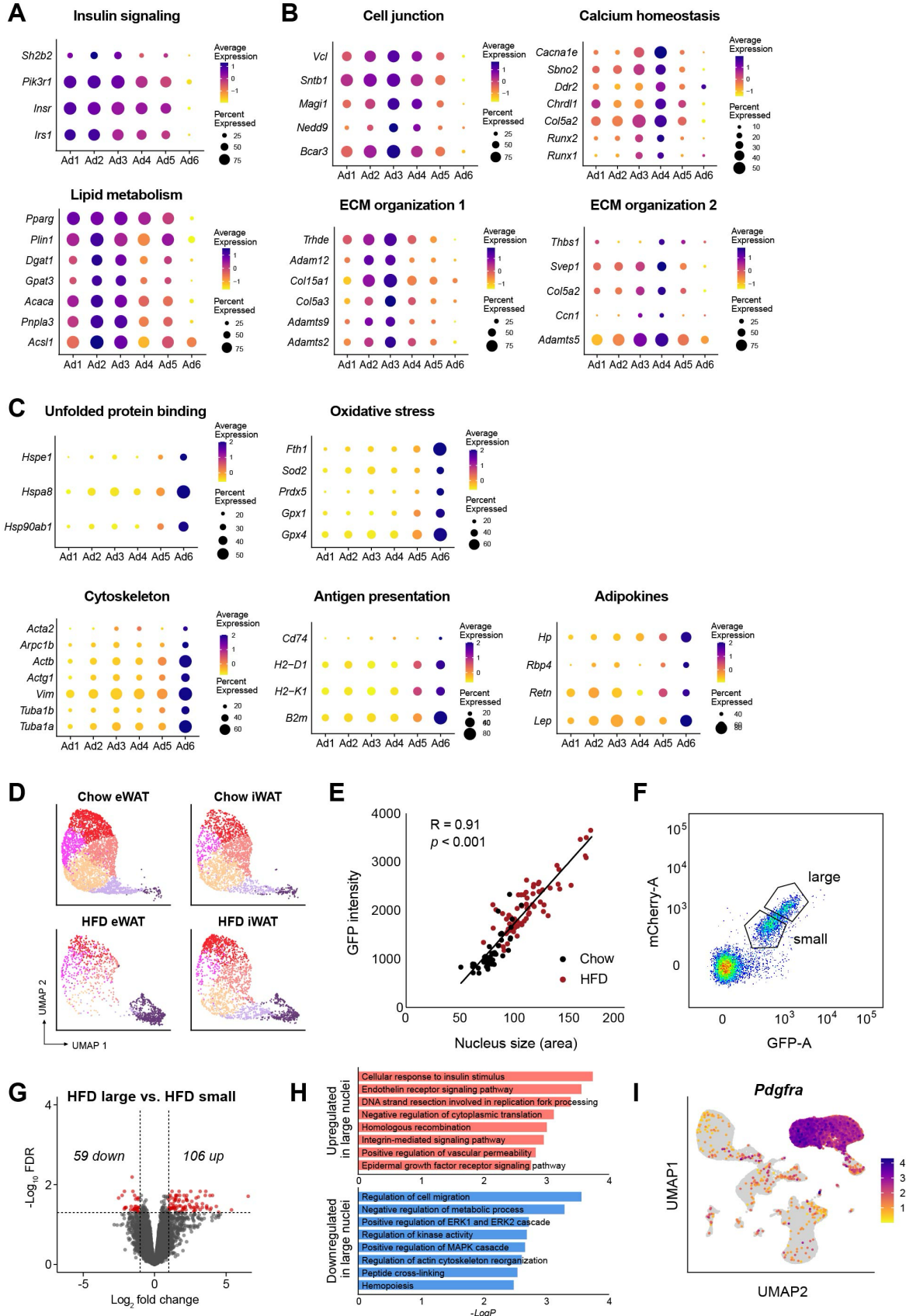


Figure S6. Identification of functional attributes of adipocyte subpopulations. (A-C) Dot plots representing the expression of genes linked to distinct biological processes enriched in different adipocyte subpopulations: **(A)** for Ad1-2, **(B)** for Ad3-4, and **(C)** for Ad6. **(D)** UMAP plots of adipocyte subpopulations by fat depot and diet. **(E)** Correlation between nucleus size and GFP intensity in adipocyte nuclei isolated from adipose tissues of chow-fed (black) or HFD-fed (red) Ad-NuTRAP mice. P value was calculated using an F-test with the null hypothesis that the slope is equal to 0. **(F)** Sorting criteria for gating adipocyte nuclei isolated from iWAT of HFD-fed NuTRAP mice into small and large nuclei. **(G)** Volcano plot showing statistical significance ($-\log_{10}$ FDR values) versus fold change of gene expression between large and small adipocyte nuclei from iWAT of HFD-fed mice. Red dots represent genes that were differentially expressed between groups with an FDR < 0.05 and $|\log_2$ fold change| > 1. **(H)** Bar graphs illustrating the top GO terms (GO: BP) enriched in upregulated (top) and downregulated (bottom) genes in large versus small adipocyte nuclei. **(I)** UMAP visualization of an APC marker gene, *Pdgfra*.

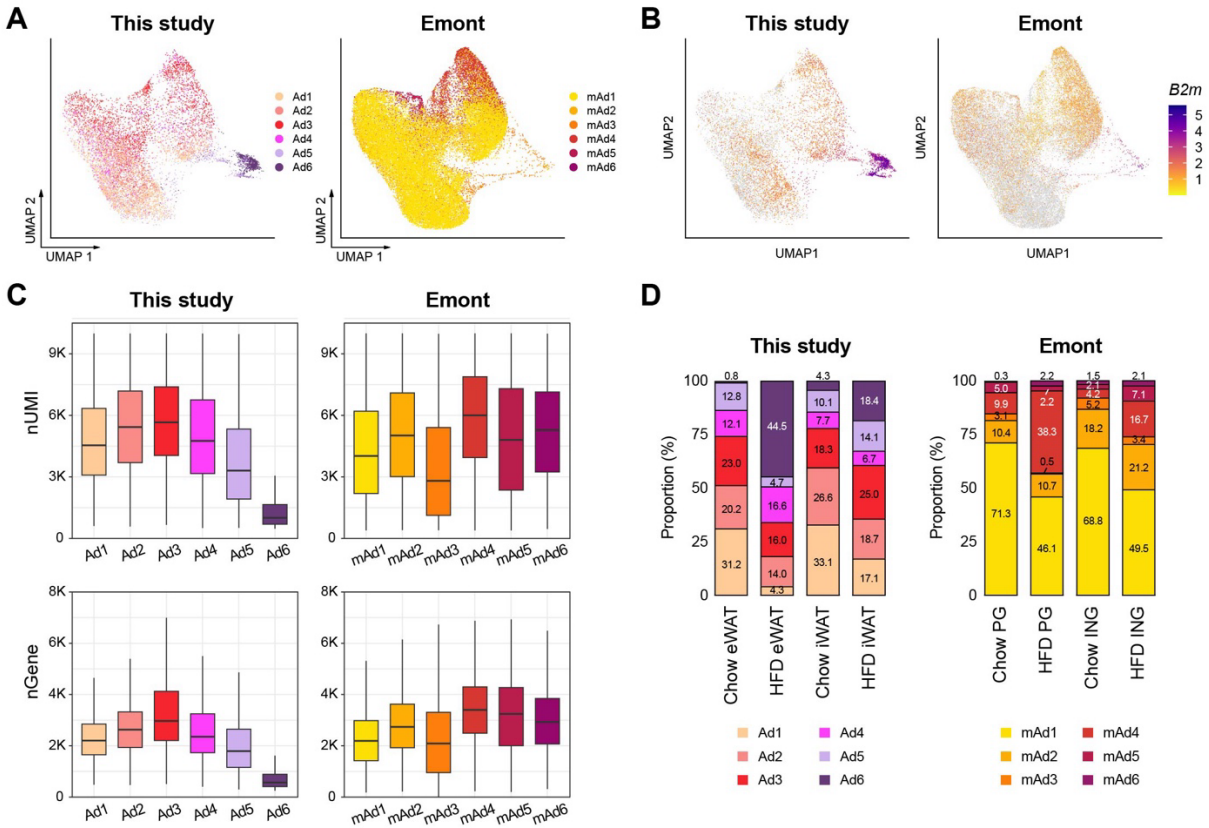


Figure S7. Comparison of adipocyte subpopulations identified in this study versus Emont et al. (A) UMAP visualization of integrated adipocyte nuclei from this study and Emont et al. **(B)** B2M gene expression in adipocyte nuclei from each dataset. **(C)** UMI counts and genes detected per nucleus by adipocyte subpopulations in this study and Emont et al. **(D)** Bar graphs displaying the relative proportions of adipocyte subpopulations identified in this study and Emont et al.

Table S2. Sequences of primers used for quantitative real time PCR (qRT-PCR).

Gene	Sequences (Forward)	Sequences (Reverse)
<i>Adipoq</i>	TGTTCTCTTAATCCTGCCCA	CCAACCTGCACAAGTTCCTT
<i>Cebpa</i>	CTGAGAGCTCCTTGGTCAAG	CGAAACCATCCTCTGGGTC
<i>Dlk1</i>	CTTTCGGCCACAGCACCTAT	CATGGCACCTGCAGACATTG
<i>Emr1</i>	CTTTGGCTATGGGCTTCCAGTC	GCAAGGAGGACAGAGTTTATCGTG
<i>Fabp4</i>	AAGGTGAAGAGCATCATAACCCT	TCACGCCTTTCATAACACATTCC
<i>Fam214a</i>	AGGCTTCCAGTATGGTTTTTCAG	AGGCCAAAGAGACCAAGAAC
<i>Pecam1</i>	CTGCCAGTCCGAAAATGGAAC	CTTCATCCACTGGGGCTATC
<i>Plin1</i>	AATGAGTTGGCCTGCAGAG	AGGCGGGTAGAGATGGTG
<i>Pparg</i>	GTGCCAGTTTCGATCCGTAGA	GGCCAGCATCGTGTAGATGA
<i>Vcam1</i>	CTGGGAAGCTGGAACGAAGT	GCCAAACACTTGACCGTGAC
<i>36B4</i>	GAGGAATCAGATGAGGATATGGGA	AAGCAGGCTGACTTGGTTGC